Chapter 1

Introduction

1.1 Background

The need to find the deformation required to morph one complex geometry into another arose from a study done on the effect of prognathism on masticatory induced stress in the human skull.

Maxillary alveolar prognathism is defined as the percentage relationship between two lines, both with origin at the cranial base (ba) and through the cranial landmark positions of nasion (n) and prosthion (pr). This attribute is characterised by either one or both jaws projecting forward, clearly influencing the general shape of the maxillofacial region of the skeleton. For the location of these landmarks see Figure 1.1.

In the initial study, a comparison is made on results obtained from a finite element analysis on two different skull geometries.

To best compare results, it would be beneficial to have a computational domain for the different skulls that have one-to-one correspondence. If this is possible, even more patient specific geometries could be analysed as part of a complete study on prognathism's effect on masticatory induced stress using domains with one-to-one correspondence.

The principal shape components within a class of geometries, or even the deformation and stress components could be extracted if the same analysis is done using a larger statistical sample with a consistent mapping between them. The difference in stress or displacement from the mean stress and deformation due to prognathism or some other mode of variation could then be compared or calculated due to the

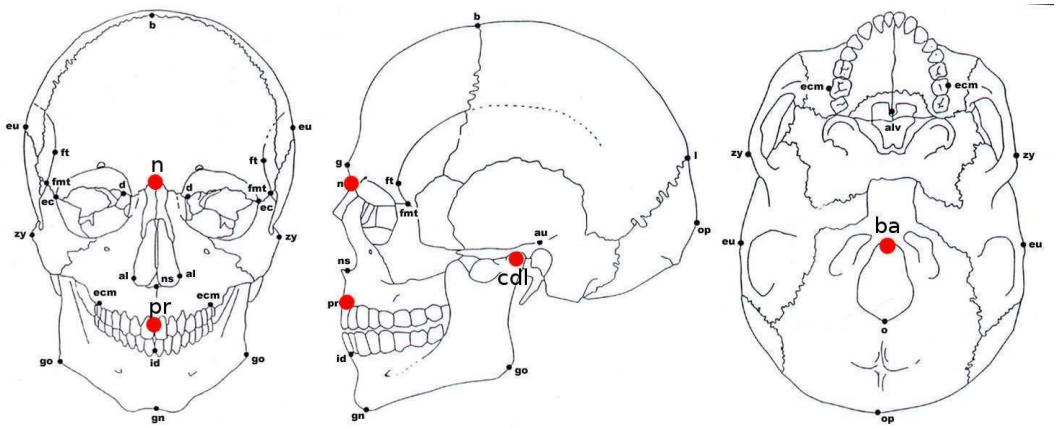

(a) (b) (c)

Figure 1.1: Landmarks on the (a) front, (b) side and (c) bottom of the human skull [43].

existence of this consistent mapping.

Unfortunately one-to-one correspondence of the computational domain generated from extracted geometries, or even alternative designs in the engineering industry, is highly unlikely. An approach to obtain a computational domain that represents various geometries with the exact same mesh size and connectivity between the nodes does however exist. This could be achieved by deforming a generic mesh into that resembling all different geometries in the sample.

This report covers an introductory study to register and deform a generic mesh (also called the base mesh, deformable mesh or model shape) into a representation of a complex target geometry or data shape. Various procedures are investigated, implemented and combined to specifically accommodate complex geometries like that of the human skull.

The procedures implemented have various aspects that still require improvement before the desired study regarding prognathism's effect on masticatory induced stress, could truly be approached pragmatically. Focus is only given to the use of existing procedures while the additional required improvements could be addressed in future work. It is however required that the resulting discretised domain obtained in this initial study be of sufficient quality to use in a finite element analysis (FEA) [24].

1.2 Outline of Thesis

1.2.1 Chapter 2: Background Work and Problem Statement

The background work involves performing a finite element analysis (FEA) on two skulls. A prognathic and non-prognathic skull form is selected from the University of Pretoria's skull collection. Computed tomography (CT) scans of these geometries are used to construct surface mesh representations. The surfaces are then edited and smoothed before creating tetrahedral meshes for use in the aforementioned FEA. Masticatory induced stress is determined for a bite force on the first molar and first incisor. Resulting stress fields on the different geometries analysed are then compared.

Problems are discussed in drawing conclusions on the resulting stress field due to differences in the analysed geometries. The geometries analysed seem to differ in more ways than prognathism alone. Differences in these geometries are especially visible when comparing the sinuses and internal features. The latter could be as a result of decay.

Suggestions are made on how prognathism's effect on masticatory induced stress could be inspected better. The variation in stress due to prognathism alone would probably require the use of a larger sample of geometries. If it is then possible that a single mesh can be used to appropriately represent the different skull geometries by only updating nodal coordinates, a more rigorous analysis on the variation in stress field due to prognathism can be performed.

Principal modes of variation in human skull geometry can be obtained from a principal component analysis (PCA) [36] on the large data set. Each data shape is represented with different nodal coordinates only. If one of these modes is to represent prognathism, this mode could be identified with the help of medical experts and isolated. The deviation from the stress in the mean skull shape due to this mode can then be determined to better support or contradict the hypothesis.

This hypothesis states that a different stress field is expected in the crania of a human with prognathic[1] facial form when compared to that of a human with orthognathic[2] facial form during a similar cycle of mastication. Bone adapts to mechanical needs and different skull geometries are therefore expected to undergo thickening in different locations.

[1] One or both jaws projecting forward.
[2] Jaws don't project forward giving a flatter facial profile.

The remainder of the project is focused on investigating the possible registration and deformation of a generic skull geometry to better represent a new target data shape.

1.2.2 Chapter 3: Elastic Surface Registration

Deforming a generic surface into a target configuration is done using elastic surface registration. In the procedure implemented for this report, this involves finding and reducing the difference between two surfaces.

The closest distance form every point on one surface to that on the opposite surface may be used as a similarity measure. Firstly, issues related to a difference in the target and generic shape orientation and scale is addressed. It is then possible to deform the generic surface into a representation of the target shape.

The generic to target closest distance directions and inverse of the target to generic closest distances are used. A deformation field is determined with Gaussian weighted smoothing and applied to the generic mesh. This process is performed iteratively until some requirement on the similarity between the deformed and target mesh is satisfied or no further improvement is possible.

Full registration with the implemented procedure could have undesired results when applying it to a geometry as complex as the skull. The use of feature based registration as an initial deformation before elastic surface registration is mentioned and investigated.

1.2.3 Chapter 4: Geometric Features

Extracting curvature information from a discretised surface representation is investigated and discussed. Areas of the surface can be classified as possible feature rich areas or flat surfaces using this local curvature variation.

Feature points, ridges and valley lines on the surface mesh are automatically extracted. The use of these features in the implemented feature based registration is discussed in Chapter 5.

1.2.4 Chapter 5: Feature Registration

There are different methods that could be used to deform a generic mesh into that closely resembling a target geometry. Varying methods differ in complexity and the

final accuracy with which they resemble the target. Some of these feature based methods and their usual applications are investigated. The use of landmark points as well as feature lines are discussed.

Landmark Nodes

The simplest method involves manually defining landmark nodes on the generic mesh. The landmarks on other geometries can be obtained by either marking it on the digital geometry or by using a digitising stylus. Alternatively, methods exist to extract and classify landmarks by using differential geometry and shape context histograms.

If a relationship between target and generic landmark coordinates is found, the target coordinates can be scaled, translated and rotated so that the distance between corresponding landmarks are minimised in a least squares sense. The displacement required to deform the generic landmark coordinates into the target configuration is then determined. This displacement is applied using radial basis functions or another mesh movement method to deform the rest of the mesh into an approximate target configuration.

Feature lines

Feature lines can be extracted from surface meshes by applying differential geometry principles. Feature lines or parts thereof on a target shape can be compared with those on a generic surface mesh in order to find possible equivalents. Rigid body movement and a scale factor is applied to the target feature lines. This is done so that the generic features are matched in a least squares sense.

Various techniques can be used in determining the deformation required from the generic to target feature lines. The displacement from an original generic line to the deformed state can be determined. With nodal displacements known, a mesh movement method can be applied to the generic mesh to deform it into an approximate target configuration.

The use of feature lines as an initial coarse registration is implemented and investigated before applying the elastic surface registration procedure. Improved results are obtained for the creation of a symmetric skull from an edited and smoothed mesh compared to the original attempt where feature lines weren't used. Figure 1.2 illustrates the basic concept of combining feature based registration with elastic

surface registration to deform a generic mesh into a target representation.

Registering a new complex target shape could still present a few problems. This is addressed in the proposed registration procedure. In the proposed combination of procedures, unmatched feature surfaces are automatically discarded prior to surface registration. Higher confidence areas are used in combination with user-selected allowable regions of the surface in an attempt to improve the registration result.

1.2.5 Chapter 6: Proposed Registration Procedure

The proposed registration procedure is a combination of an implemented elastic surface registration and feature line registration procedures. The feature registration is done before surface registration to find matching features. Unmatched features are seen as a possible difference in topology between the generic and target geometry. The reason for this is that an unmatched feature line could possibly be due to a hole in one volume with no equivalent hole in the other.

Features are expanded to contain not only the thresholded lines of curvature, but entire feature surfaces. Registration to an unmatched surface is simply ignored during elastic surface registration. As an example, feature registration is done using only user selected features on the assumed generic skull surface. The unmatched features and associated feature areas on the target can be automatically discarded to reduce the amount of editing needed before registration. This procedure in conjunction with additional user constraints on allowable surfaces are inspected. The procedure still requires further attention on the uniqueness of a registration result for use in eventually registering a larger set of skull geometries.

The Department of Anatomy at the University of Pretoria is in the process of creating a digital database from the skulls in their possession. In future, the registration could be performed on a statistical sample of these geometries. The variation in stress field attributed to individual modes of geometric variation can then be analysed.

The benefits of having meshes with one-to-one correspondence is illustrated in a few examples. This is done with registered representations of the two human skull geometries used in the initial analysis. An FEA is done on symmetric versions of these skulls. By deforming a skull mesh into that of it's mirror image, a symmetrical skull is simply obtained from the average between the original and deformed configuration. The deviation from symmetry in the skull is then removed and the

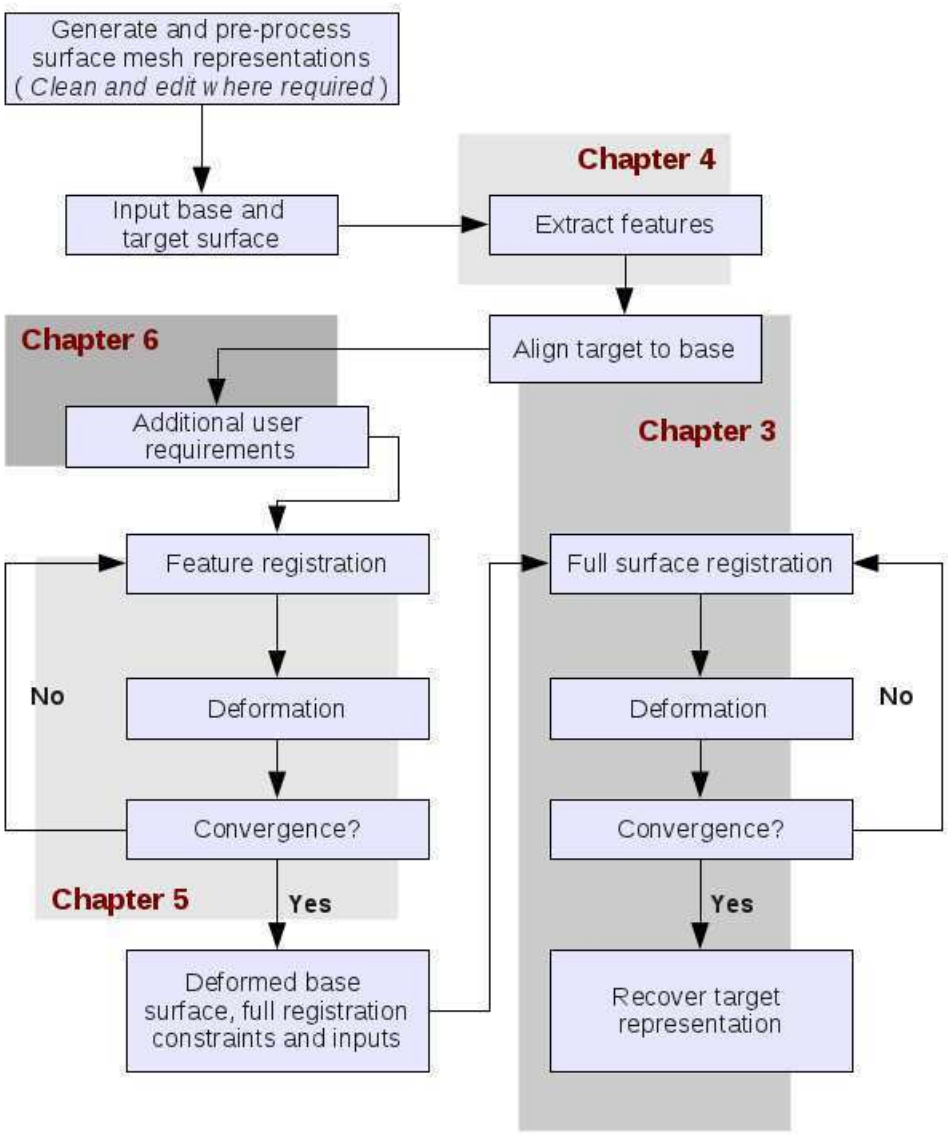

Figure 1.2: Flow diagram illustrating the basic idea of combining feature and surface registration. In the implemented procedure, the result of the feature based registration is used as input and also dictates allowable surfaces used during surface registration.

stress variation due to this asymmetry can be neglected. By analysing symmetric geometries, the variation in stress is more likely due to the relative degree of prognathism than due to the relative degree of asymmetry.

1.2.6 Chapter 7: Conclusions

Remarks, possible future work and the possible use and application of a reliable registration procedure are discussed in Chapter 7.

Chapter 2

Background Work and Problem Statement

2.1 Introduction

The forces applied through the cycles of mastication are influenced by a variety of factors. The size and strength of masticatory muscles and their attachment to structures within the crania are of importance. The size and form of cranial structures and the location of healthy teeth and gums also have major influence.

To simulate mastication and determine the corresponding stress field, a finite element model can be created and analysed from a digital patient's cranial geometry. This includes decisions made on the appropriate material properties, boundary conditions and imposed loads.

The background work aims to apply the general rules of bone behavior and muscle activity in order to test a hypothesis about a single facial characteristic and is done in collaboration with a Ph.D. student in Anthropology.

The hypothesis of the Ph.D. work states that the location of bone stress in the crania of a prognathic facial form will vary from that in the orthognathic facial form. An attempt to test the hypothesis with the aid of a finite element tool is done with this in mind.

An account of how material properties and boundary conditions are set up in the finite element model for each skull is covered in Appendix A along with some results on the finite element analysis. A broad overview of the initial work done for this study is given in this chapter. This is accompanied by conclusions on how elastic

registration could help in finding the change in a masticatory induced stress field due to a change in prognathism. If a large enough statistical sample of geometries can be represented with the same mesh, a principal component analysis (PCA) [36] could recover the mode of variation closely linked to prognathism. The variation in stress field due to this mode could be quantified once it is isolated.

2.2 Prognathism in the human skull

Evolutionary biologists and dental practitioners are interested in the history and study of sub-nasal maxillary alveolar prognathism. This attribute is characterised by either one or both jaws projecting froward, influencing the general shape of the maxillofacial region of the skeleton. Upon visual inspection, this is one of the most noticeable morphological characteristics of the human skull.

Maxillary alveolar prognathism is defined as the distance ratio between two lines. These lines both have their origin at the cranial base (ba) and connect this point to the cranial landmarks of nasion (n) and prosthion (pr) positions [14]. The location of these landmarks are highlighted in red on Figure 1.1.

Expressed as a percentage quantity, the distance ratio is termed the gnathic index (GI) and is defined as

$$\mathrm{GI} = \frac{\|\mathrm{pr} - \mathrm{ba}\|}{\|\mathrm{n} - \mathrm{ba}\|} \times 100. \tag{2.1}$$

This index is also termed the alveolar index. Skulls with a gnathic index below 97.9 are orthognathous. Mesognathous skulls have an index between 98 and 102.9 while prognathous skulls have a GI value above 103 [53].

In the study of geometric morphology[1], statistical correlations have been found between various cranial characteristics in modern human skulls. Research has found that prognathic individuals have longer jaws in relation to their cranial base length along with other geometric characteristic [18, 63]. The crania itself is flatter and the foramen magnum[2] is positioned further back. With a decrease in the degree of prognathism, the jaws shorten accompanied by a forward movement of the posterior region of the cranial base. The prognathic facial form can also be linked to a short and lower face height, longer posterior upper, an increase in orbit height and

[1] Statistical analysis of form based on Cartesian landmark coordinates.
[2] Where the spine articulates with the cranial base.

decrease in orbital breadth [18, 63].

2.3 Mastication

If a prognathic and non-prognathic skull were scaled so that the distance from the jaw hinge to the site of effective muscle attachment is the same, these muscle forces in the prognathic form would have to be larger than that of the non-prognathic form to exert the same incisal bite force. This is due to the relative distance from the jaw hinge and muscle attachments to the position of the applied bite force.

The masticatory system is made up of various bone structures, muscle fibres and other tissue types with a wide range of differing properties and effects. When using an FEA toolkit to simulate mastication, the detail with which these material properties and boundary conditions are modelled could dramatically affect the accuracy.

Attention is given to previous studies where mastication is simulated using primate skull geometries. The mandible, which is attached to the skull itself through the temporomandibular joint (TMJ), acts as a lever during mastication. The distance from the bite force on the tooth to the TMJ (approximately at the (cdl) landmark in Figure 1.1) and the relative muscle attachments result in a different applied force for the prognathic and orthognathic skull form.

2.3.1 Teeth

The forces of mastication change in magnitude throughout the dental arcade. Posterior teeth where the larger possible bite force occurs have a greater occlusal surface area. The location of the molars in closer proximity to the masseter and medial pterygoid muscles create a greater force at this location [48].

The periodontal ligament and alveolar bone surrounding the teeth at the load bearing point also dictate what force is exerted. Using a feedback loop from receptors that monitor stress, teeth are protected from potentially damaging forces [46].

2.3.2 Bone

Like other tissues, bone has the ability to change and repair. It functions as the framework for mobility and also acts as support, protection and the body's calcium

reserve. Bones contain the cells responsible for bone formation (osteoblasts) and bone resorption (osteoclasts). During remodelling, osteoblasts deposit bone as a result of high strain while osteoclasts reabsorb bone due to decreased strain signals [66].

Specific adaptations in bone morphology vary throughout the skeleton. This depends on the composition of compact and cancellous bone, anatomical location and the specific function of a particular bone. Cancellous bone is first to react to the change in mechanical needs and undergoes a greater change in density while cortical bone experiences prolonged change [56].

Bone structures in the craniofacial area serve in part to accommodate and support the stresses created during the cycles of mastication [67]. A particular study [55] focused on temporal bone variation subject to climate changes. In this study Smith *et al.* noted that neural evolution and mechanical stresses caused by the availability of certain foods also played a role in the observed variation.

Some researchers have claimed that the roll of mastication forces acting on the skull dictates skull shape more than any other external force [49]. The muscles of mastication change with force and intensity and the skull is thought to be optimised to meet the mechanical needs during feeding. The skull is presumably thicker in certain areas to accommodate masticatory induced stress.

The variation in stress due to prognathism in the facial form is therefore assumed to result in a difference in bone mass within certain areas of the facial structure.

2.3.3 Muscles

Masticatory muscles have corresponding skeletal attachments on the skull, maxilla, and mandible. Each of these muscles act on the underlying bone to create a required bite force.

The strength with which muscle forces are applied is dictated by several factors. Some of these factors include muscle fibre length, sacromere length and the directional orientation of the fibres themselves [16]. The temporalis muscle, masseter muscle and medial pterygoid are used in the elevation of the mandible [30]. These muscles act on the mandible during the cycles of mastication and are modelled in this report. The masseter muscle is divided into the deep and superficial portions. The approximate position of the muscles modelled are described below with reference to Figure 2.1:

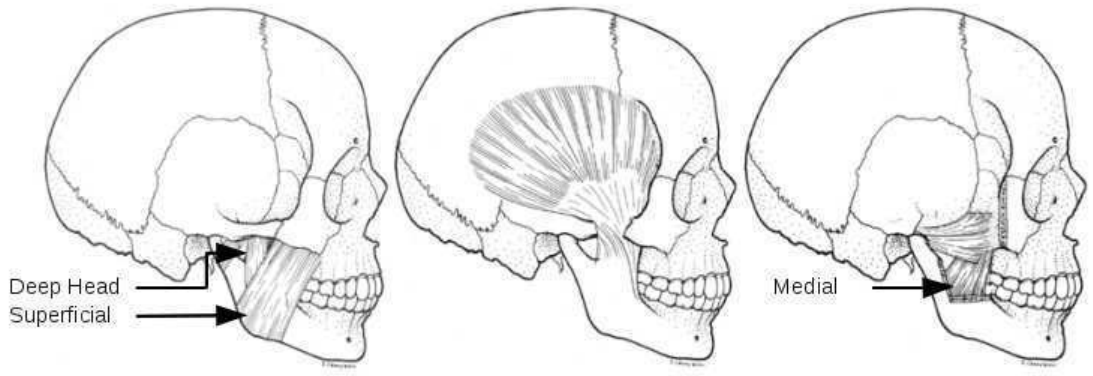

(a) (b) (c)

Figure 2.1: Masticatory muscles [12]. (a) Masseter, (b) Temporalis and (c) the lateral and medial Pterygoid.

- The superficial masseter originates at the anterior and inferior $^2/_3$ margin of the zygomatic arch and inserts at the angle of the mandible. This muscle is the front most muscle visible in Figure 2.1 (a)
- The deep head masseter originates on the posterior $^1/_3$ of the medial surface of the zygomatic arch and inserts at the ramus of the mandible [30]. This muscle is illustrated as the two sections of the inner muscles visible in Figure 2.1 (a)
- The temporalis muscle characterised by its fan shape encompasses the temporal fossa on the lateral sides of the skull and inserts on the coronoid process of mandible. It is divided into an anterior portion and shallower posterior region [16, 30]. This muscle and it's attachment to the mandible is visible in Figure 2.1 (b)
- The medial pterygoid muscle used in jaw elevation has an origin at the pterygoid fossa of the sphenoid bone and inserts at the angle of the mandible on the medial side [30]. The lateral pterygoid is the muscle that attaches at the TMJ position in Figure 2.1 (c) with the medial pterygoid attached lower on the mandible.

2.4 Finite Element Model

A brief overview of the finite element model used in analysing the two skull forms for masticatory induced stress field is given in this chapter while the reader is referred

to Appendix A for additional detail.

2.4.1 Geometries

Considering that the reason for this study is a validation on the adaptation of skull form to minimise internal stress due to mastication, two skulls were selected for analysis based on gnathic index and sufficient dentition from the University of Pretoria skull collection [39]. A skull with a gnathic index of 106.9 is used to represent a prognathic facial form and a skull with a gnathic index of 91.5 represents the orthognathic facial form in the work done.

Taking into account that exact stress values aren't required and that this study is mainly concerned with the variation in stress pattern, a four noded tetrahedral finite element mesh was created from the digital surface representation of these skull forms using TetGen [9].

2.4.2 Material Properties

Significant variation in material properties have been documented for a range of different bones and within different areas of the same bone structure [47]. The anisotropic nature of bone and how to model it however is not the focus of this research.

Tetrahedral finite element meshes were imported into PreView [7] to set up the model. This is done by defining material properties and boundary conditions. For similar analyses done in literature, isotropic bone material properties have been reported to produce realistic stress patterns [17, 20, 32, 35, 38, 60].

The Young's modulus and Poisson's ratio used in this study was taken from literature to be 16 GPa and 0.3 [17, 20, 32, 35, 38, 50, 60].

2.4.3 Boundary Conditions

FEBio [3], a solver developed specifically for biomechanic finite element applications is used in performing this study. Although this allowed for muscles and tendons to be modelled using an array of element types, it was decided that the forces of mastication would be modelled as external forces on the available skull geometries. These forces are applied to nodes in the region representing the approximate sites of muscle attachment described previously with the help of Figures 2.1 and 2.2.

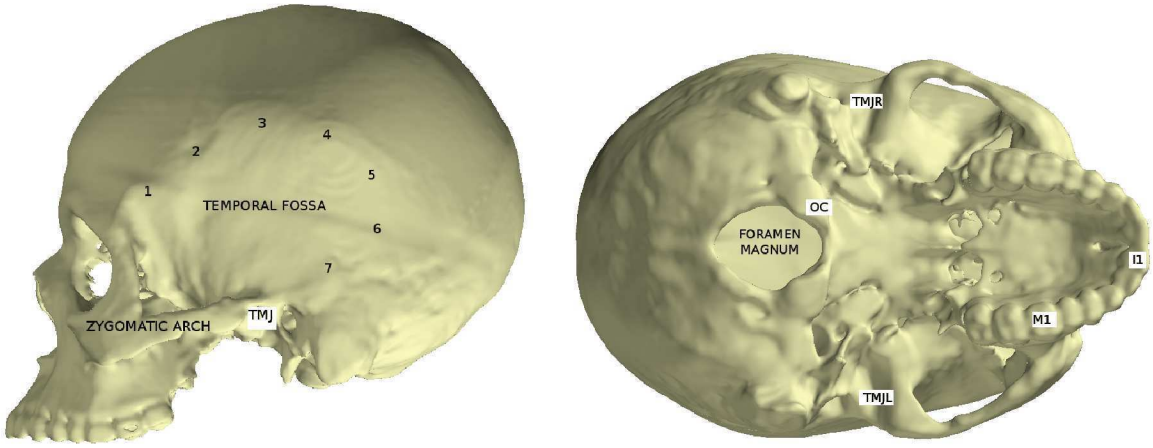

(a) (b)

Figure 2.2: Boundary condition positions on the skull. (a) Lateral view of the prognathic skull indicating the Temporal fossa and zygomatic arch (cheek bone). The jaw hinge or temporomandibular joint is indicated by TMJ and the seven sections of the temporalis muscle attachment positions are indicated by numbers 1 through 7. (b) Inferior view of the prognathic skull. The location of boundary constraints are the occipital condyles (OC) on the foramen magnum. Reaction forces are determined at the left and right temporomandibular joints (TMJL and TMJR) and either the first molar (M1) or first incisor (I1) for the applied muscle forces when balancing the system.

Muscle force values are first approximated for a vertical bite force on the first incisor and first molar. These teeth are visible as I1 and M1 in Figure 2.2. Muscle action during the cycles of mastication are different for working and balancing sides. For this stress simulation the left side of the skull is chosen as the working side of the dental arcade where bite force is applied. Here force values used are determined from literature [64] while force scaling factors on the right side are obtained from a study on muscle activity during mastication [57].

Mastication is an internally balanced system. Keeping this in mind, a system of equations is set up and solved to obtain the bite force at the tooth and reaction forces at the temporomandibular joint (TMJ) for each skull model. In doing so a number of assumptions are made and the problem is considered as a rigid body under static loading. The model was constrained in the region of the foramen magnum at the occipital condyles in all six degrees of freedom to prevent rigid body movement. These locations on the skull and an accompanying short description is also visible in Figure 2.2.

For further information on setting up and solving the system of equations, as well as a free body diagram, the reader is referred to Appendix A and Figure A.1 in particular.

Both skulls are treated similarly and several finite element analyses were run for both incisal and molar bite using FEBio [3]. Muscle forces with their balancing reaction forces are applied as boundary conditions with the nodal coordinates of the occipital condyles at the foramen magnum constrained. Figure 2.3 shows the applied muscle forces and reaction forces obtained for a full molar bite in such a way that the system is balanced for both prognathic and orthognathic skull form.

Post processing and visualisation is done using PostView [6]. Using the boundary conditions obtained from the static analysis displayed in Figure 2.3, the results of a linear elastic finite element analysis on these skull forms for a molar bite can be seen in Figure 2.4 (a) and (b). The full incisor bite resultant Von Mises stress field is also visible in Figure 2.4 (c) and (d) with further examples in Appendix A.

2.5 Results

Comparing the results of the finite element analyses on the two skull forms present a few problems. These skull forms could have other differences in form not correlated to only the gnathic index. This is undesired when drawing conclusions on the effect

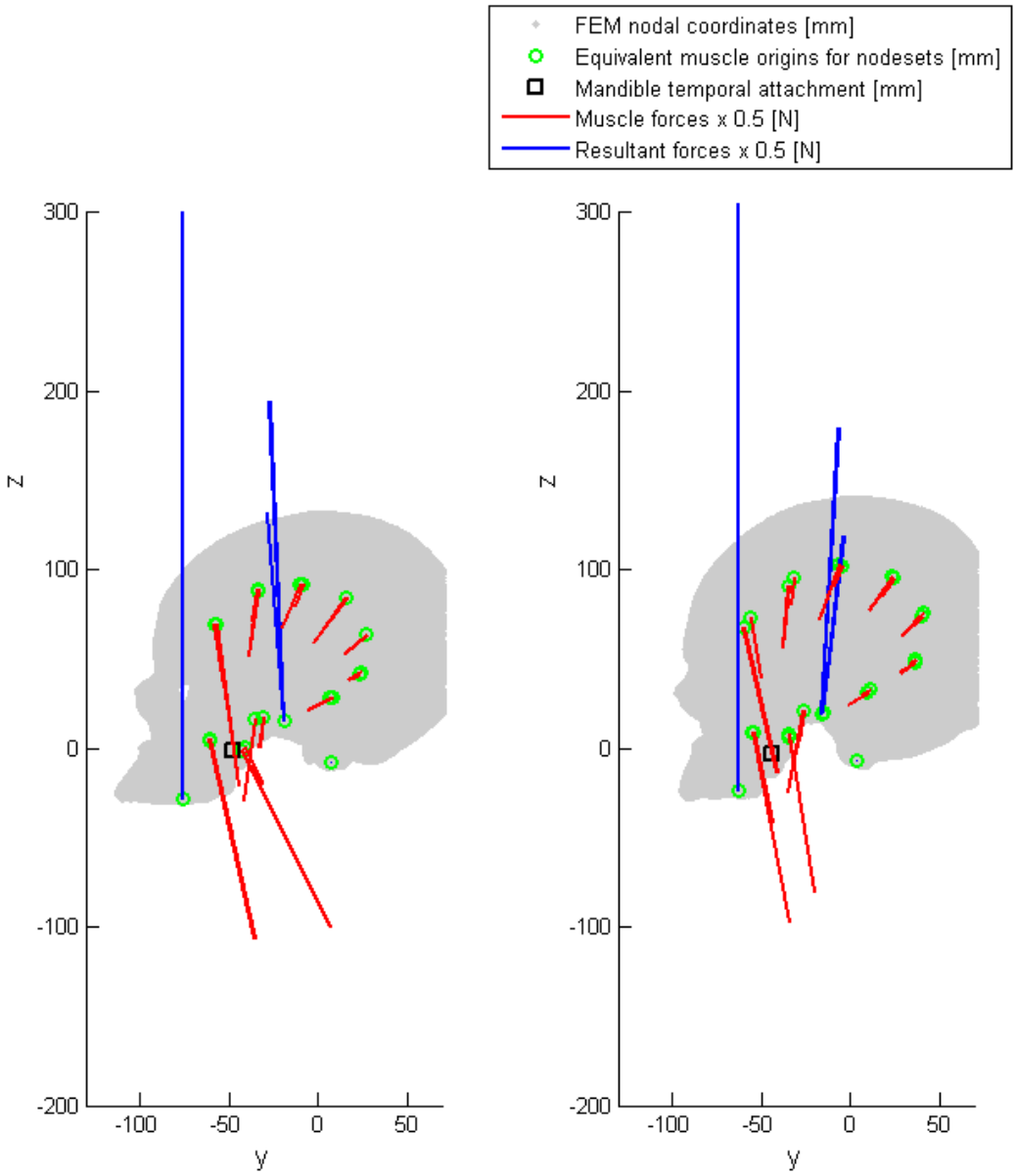

Figure 2.3: Muscles and reaction forces on (a) the prognathic skull form and (b) orthognathic skull form for a vertical molar bite.

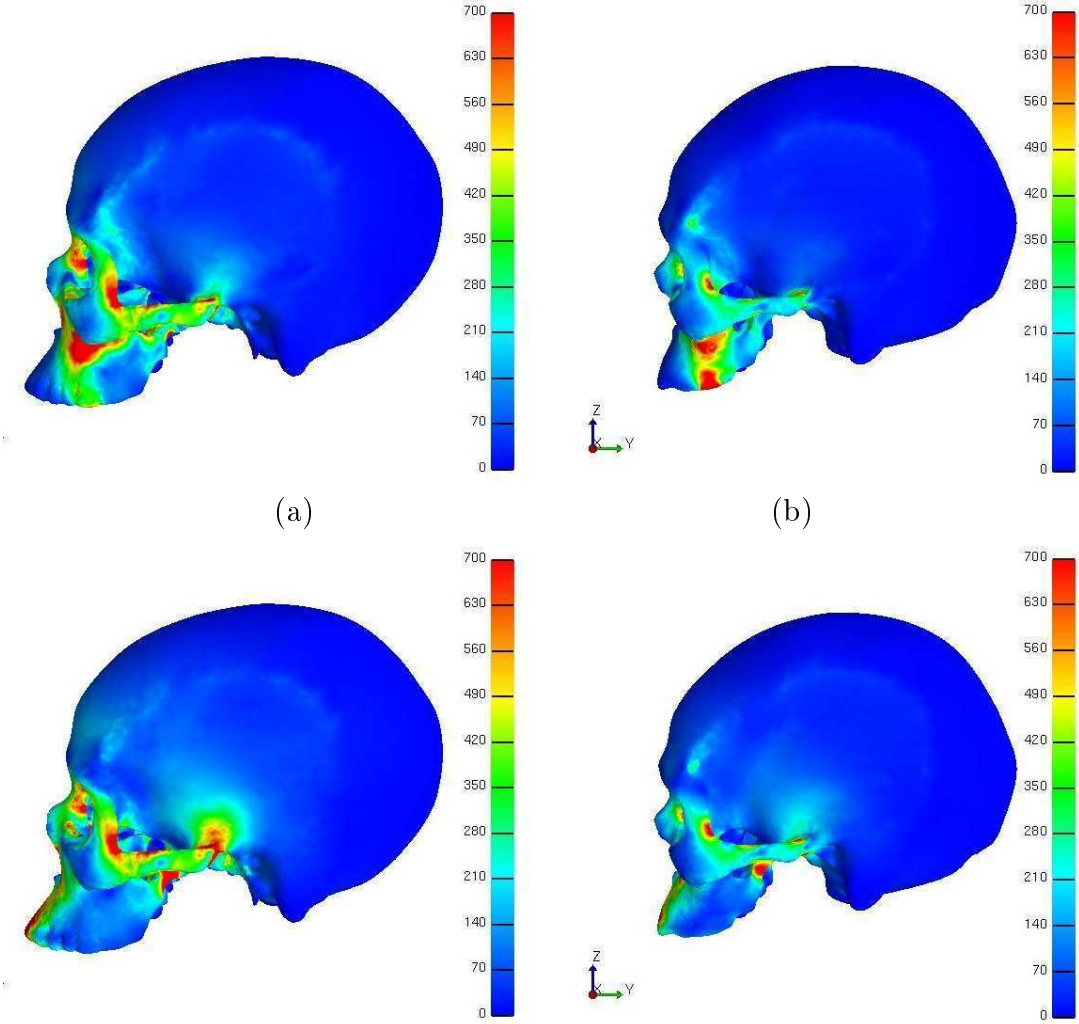

Figure 2.4: Lateral view of the working side Von Mises stress for a molar bite on the (a) prognathic and (b) orthognathic skull form as well as for an incisor bite on the (c) prognathic and (d) orthognathic FEA. The units of the stress contours are in N/cm^2.

(a) (b)

Figure 2.5: Semi-transparent view of the (a) prognathic and (b) orthognathic skull form.

of only prognathism on the resultant masticatory stress.

The skull geometries used vary in more ways than is desired. Due to decay and the presence of features or bone volume in one skull that is not present in the other, an unbiased comparison can't be ensured. Some of these differences in the original geometries are illustrated in Figures 2.5 through 2.7.

In Figure 2.5, the skull forms are displayed with semi-transparency. Despite the difference in the presence of teeth, the sinuses are seen to have vastly different form and volume. Figures 2.6 and 2.7 show cuts made through the geometry to view the boundary surfaces. From these cuts it is visible that although these skull forms are shaped differently in areas as expected, they seem to have endured varying bone loss in different areas.

To do the finite element analyses in this chapter, the skull geometries have been processed, cleaned and smoothed manually and independent of one another. For this reason it is possible that additional variation between the geometries could also be present due to slightly different fixing and smoothing strategies. In addition, the current results can only be compared visually, which is an unfortunate problem. A more rigorous comparison could be obtained if it is possible to have the same mesh

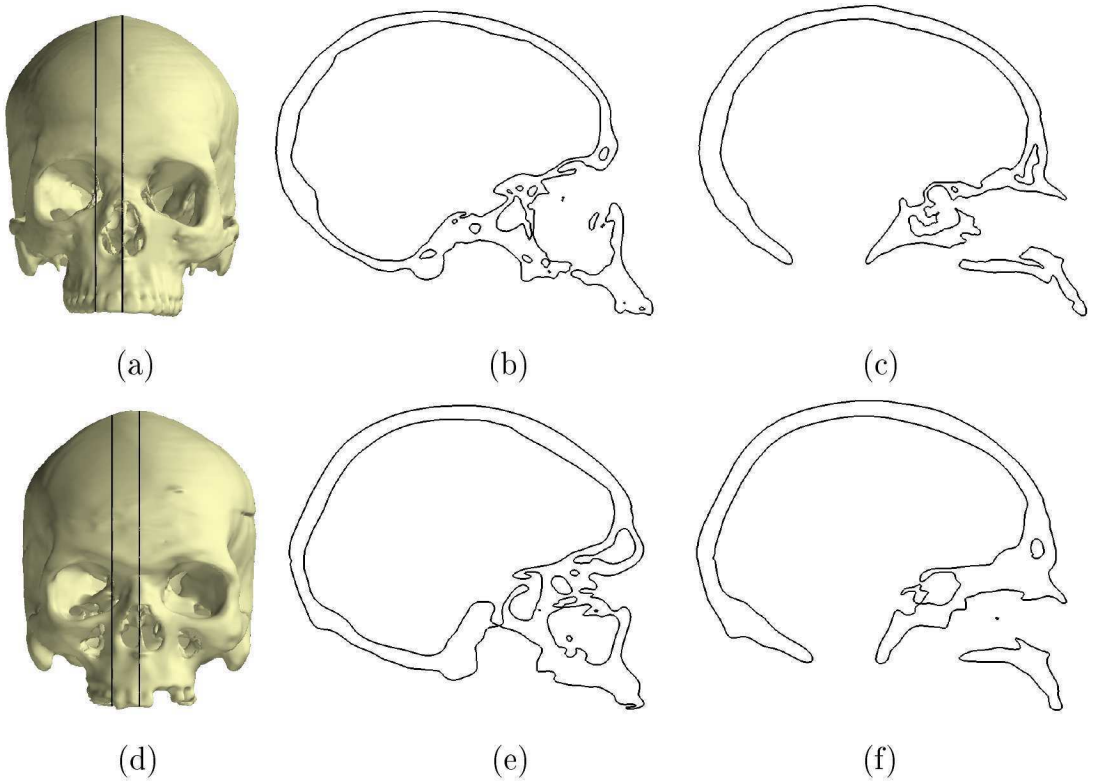

Figure 2.6: Lateral cut views through the two skulls to illustrate the difference between their boundary surfaces. (a) Location of the cut planes in (b) and (c). (d) Location of the cut planes (e) and (f).

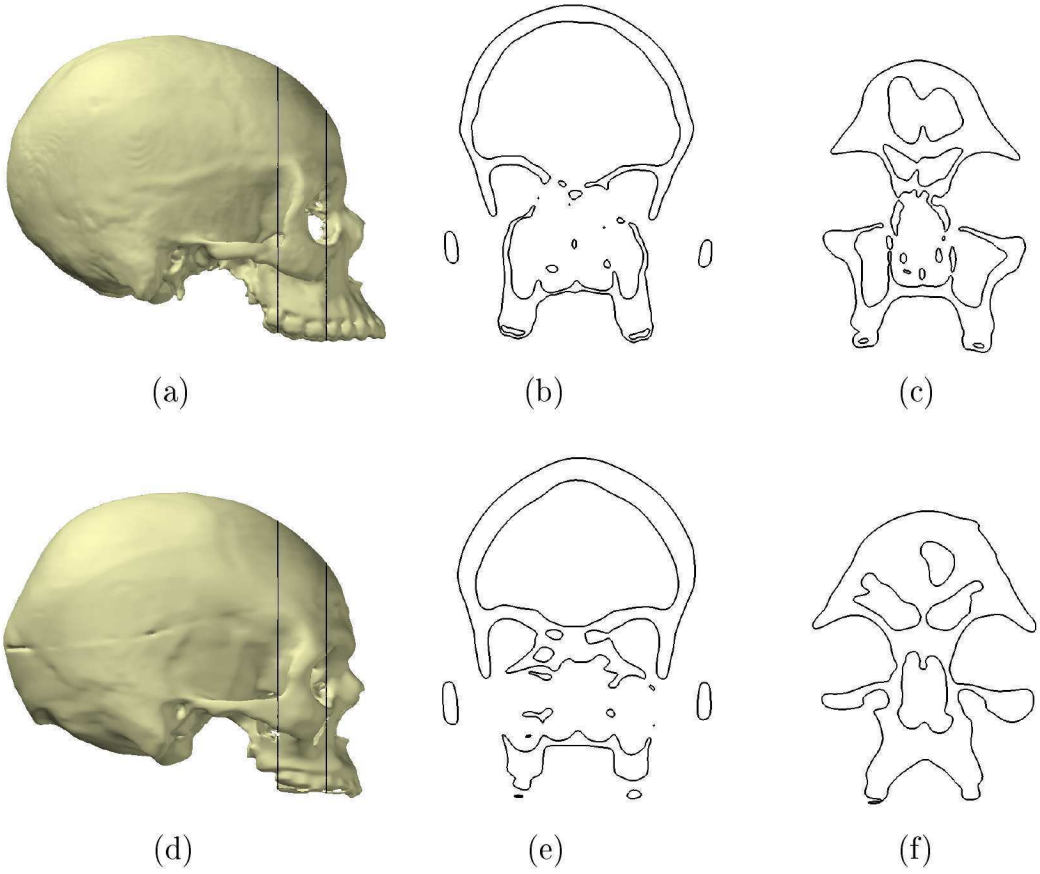

Figure 2.7: Frontal cut views through the two skulls to illustrate the difference between their boundary surfaces. (a) Location of the cut planes in (b) and (c). (d) Location of the cut planes (e) and (f).

analysed with only updated nodal coordinates to represent the difference in form.

Similar work on comparing different geometries have been performed. In Bryan *et al.* [19] for example, 46 femur geometries were modelled using the same updated mesh. From these 46 training geometries, a statistical model ready for use in a finite element analysis was created. Inter-patient variability was illustrated as the principal components of shape and variable material property. The first three modes of variation obtained in their experiments in form and material property are illustrated in Figure 2.8.

Stress and strain fields resulting from finite element analyses on such registered geometries or variation in stress due to a specific principal mode of variation could also be done. Based on the problems and shortcomings in comparing the finite element results in the initial work, it was decided that the rest of the work for the author's masters degree be approached as an introduction into elastic registration.

Again referring to Figures 2.6 and 2.7, it appears that the prognathic skull has lost more internal detail than the orthognathic skull while other features present in the prognathic skull have no equivalent in the orthognathic skull. This vast difference restricts the accuracy with which one skull could be deformed to represent the other geometry.

2.6 Problem Statement

The development of a tool for use in obtaining a better result to conclude or inspect the validity of the hypothesis stating prognathism's effect on masticatory induced stress is sought. Adequately deforming a generic skull shape into that of a different patient geometry should allow the registration of a statistical sample of skulls.

The use of a single finite element mesh with different nodal coordinates to represent each data shape in the statistical sample would be of great use. If this is achievable, all shapes in the sample set can be represented by simply updating the nodal coordinates of the generic mesh. The baseline mesh could then be created using the mean nodal coordinates and an analysis on the mean skull form could be used as the baseline stress field.

Doing a principal component analysis[3] (PCA) on the registered coordinates of the statistical sample would produce the principal modes of variation in this set. If

[3]Statistical analysis to determine the principal modes of variation in a data sample [36].

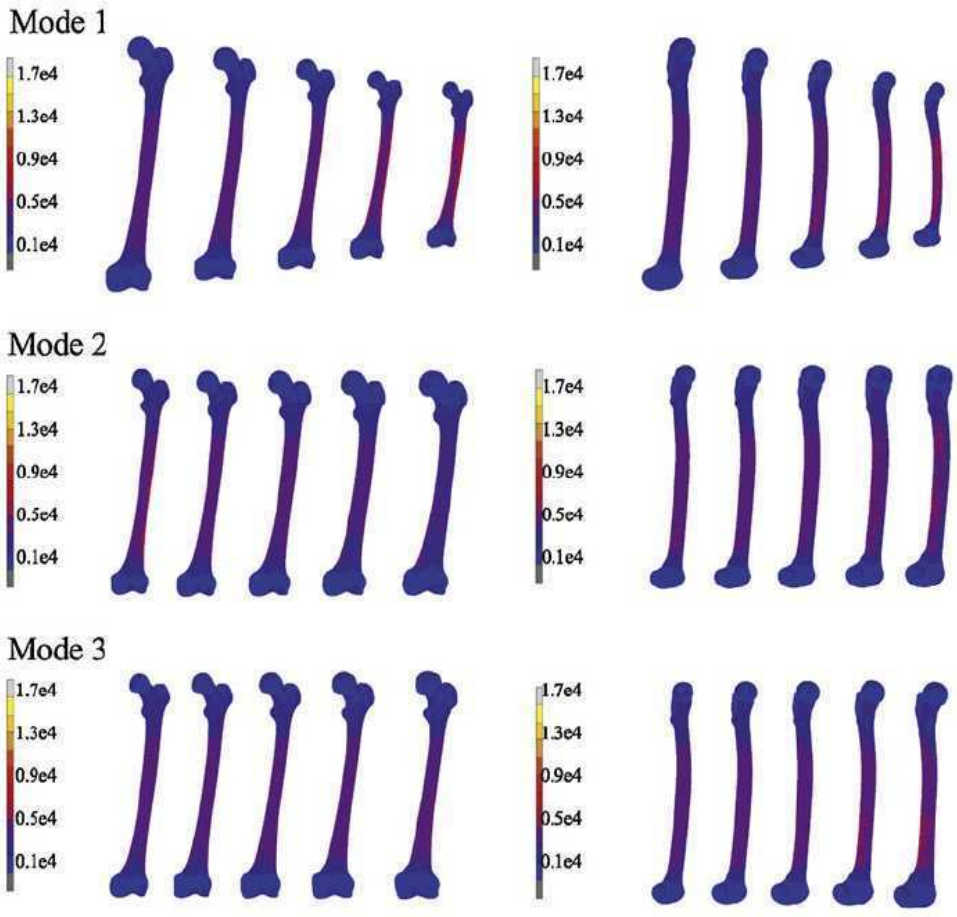

(a) (b)

Figure 2.8: First three modes of a principal component analysis done on the human femur varied between ±3 standard deviations. This is done after 46 different femur geometries are represented using the same mesh with only updated nodal coordinates [19]. (a) Frontal and (b) lateral view.

a principal mode of variation in the group of skulls is linked to prognathism, the affect of this mode on the baseline stress field can be obtained to either support or disprove the hypothesis.

The aim of the work done in the development of a tool for elastic surface registration on skull geometries are outlined:

- A deformed version of the chosen generic skull mesh should adequately represent the target geometry for use in a finite element analysis.
- Different form representations should be obtained with as little user input as possible.
- Scale effects should be taken care of as far as possible if only a few skulls are available. When comparing the stress variation between two skulls for example, it is undesired that the variation be attributed to a difference in scale. If many skulls are available this would not be a problem. Performing PCA on a larger statistical set of related geometries should isolate scale as one of the principal modes of variation. Scale is visible as the first mode of variation in the sample of femur geometries in Figure 2.8.

Chapter 3

Surface Registration

When matching a reference geometry onto a target geometry it is important to firstly take into account their difference in scale and orientation. After a rigid registration is performed, a consistent deformation of the generic geometry is required to best represent that of the target.

A selected registration technique is discussed in this chapter. This is done aimed at deforming an unstructured mesh of complex geometry into a target configuration by only updating nodal coordinates. The final goal of the registration procedure is to deform a generic digital patient geometry or atlas into that of others in a statistical set. With this in mind the difficult subject of closely similar geometries with slightly different topology is also addressed and investigated in subsequent chapters.

Rigid registration is first discussed using a modified iterative closest point (ICP) procedure reformulated from the original method proposed by Besl and McKay [13]. After aligning the target geometry with a generic mesh, elastic surface registration is addressed as used by Bryan *et al.* [19]. In [19], 46 femur geometries were registered in an attempt to create a statistical model ready for use in finite element analysis. After successful registration, inter-patient variability was illustrated as the principal components of shape and material property.

The selected elastic surface registration procedure is applied to a few sample problems. A test case is done on two femur geometries to first inspect how one geometry can be aligned to the other using the reformulated ICP procedure. The elastic registration procedure is then applied to deform one femur mesh to represent the other by updating nodal coordinates only. The femur registration is also used

to perform an analysis on the sensitivity to user controlled parameters.

Another test case is performed aimed at creating a symmetric skull surface. This symmetric mesh is created from a cleaned skull mesh with all of the teeth present and is intended for use as the generic shape in the final registration example of this project. Problems in performing this registration procedure to obtain the symmetric smooth skull is discussed briefly. In addition, the effect of user inputs on the registration result is inspected and assumptions made on what is needed to perform elastic registration on the skull geometries.

Considering the inadequate registration on geometries of this complexity and the non-unique results produced using only the selected procedure, conclusions are drawn to investigate other registration techniques. These techniques could then be applied in conjunction with the implemented elastic surface registration procedure. The possibility is discussed to improve the surface registration by including a more formal process for feature matching and registration. The issue of obtaining a unique registration result is discussed briefly and it is decided to retain the implemented registration procedure with the same parameters as used by Bryan *et al.* [19]. Further improvement to the registration procedure to obtain optimum results could be inspected in future work and is not addressed in this report.

3.1 Point Set Registration

The registration of point sets is an important issue in pattern recognition and computer vision. One of the most common methods for rigid registration is the Iterative Closest Point (ICP) algorithm [13]. This algorithm is widely used in some form or other and has been studied and improved by many researchers.

Modified versions of the ICP algorithm attempt anisotropic scaling in addition to rotation and translation. One such method [28] is discussed in this section and implemented.

3.1.1 The Iterative Closest Point Algorithm

The problem of obtaining a rigid transformation in point set registration is approached by Besl and McKay [13] as a least squares problem. For two overlapping point sets in $\mathbb{R}^m$, a rigid registration between two $m-D$ point sets aims to find the translation and rotation required to best align a data shape to the base or generic

shape.

Suppose the data and generic shape point sets are given as $\mathcal{P} \triangleq \{\mathbf{p}_i\}_{i=1}^{N_p}$ and $\mathcal{M} \triangleq \{\mathbf{m}_j\}_{j=1}^{N_m}$. The ICP algorithm involves performing a least squares optimisation problem where an applied transformation T is sought to best align $\mathcal{P}$ to $\mathcal{M}$:

$$\min_{T, j \in \{1,2,\ldots,N_m\}} \left(\sum_{i=1}^{N_p} \|T(\mathbf{p}_i) - \mathbf{m}_j\|_2^2 \right). \tag{3.1}$$

In the original ICP procedure, this transformation is made up of a rotation matrix and translation vector so that the least squares optimisation problem becomes:

$$\min_{\mathbf{R}, \mathbf{t}, j \in \{1,2,\ldots,N_m\}} \left(\sum_{i=1}^{N_p} \|(\mathbf{R}\mathbf{p}_i + \mathbf{t}) - \mathbf{m}_j\|_2^2 \right), \tag{3.2}$$

such that:

$$\mathbf{R}^T\mathbf{R} = \mathbf{I}_m, \quad \det(\mathbf{R}) = 1,$$

where $\mathbf{R} \in \mathbb{R}^{m \times m}$ is a rotation matrix and $\mathbf{t} \in \mathbb{R}^m$ a translation vector. In performing the registration, the ICP method involves iteratively performing two steps. For a k^{th} iteration:

- A correspondence is first built up between the two point sets. The correspondence for point $\mathbf{p}_i$ in the data set is given by

$$c_k(i) = \underset{j \in \{1,2,\ldots,N_m\}}{\arg\min} \left(\|(\mathbf{R}_{k-1}\mathbf{p}_i + \mathbf{t}_{k-1}) - \mathbf{m}_j\|_2^2 \right), \quad i = 1, 2, \ldots, N_p. \tag{3.3}$$

This could be done by using a $k-d$ tree nearest neighbour search algorithm to determine the closest point on the model shape.

- A rotation and translation is then determined from

$$(\mathbf{R}_k, \mathbf{t}_k) = \underset{\mathbf{R}^T\mathbf{R} = \mathbf{I}_m, \det(\mathbf{R}) = 1, \mathbf{t}}{\arg\min} \left(\sum_{i=1}^{N_p} \left\|(\mathbf{R}\mathbf{p}_i + \mathbf{t}) - \mathbf{m}_{c_k(i)}\right\|_2^2 \right), \tag{3.4}$$

  and applied to $\mathcal{P}$ before performing another iteration.

The ICP procedure was modified by Du *et al.* [28] to perform affine iterative transformations. The transformation, T, in Equation (3.1) now consists of reflection, rotation and anisotropic scale matrices as well as a translation vector. With the translation vector easily determined and the use of lie groups and lie algebra, the

ICP problem is reformulated as in Appendix B in such a way that the optimisation problem is iteratively performed subject to 9 variables. This results in the k^{th} iteration constrained optimisation problem written in the form

$$\varepsilon = \min_{\mathbf{c}} \quad \sum_{i=1}^{N_p} \left\| \mathbf{U}_{k-1} \left(\mathbf{I} + \sum_{j=1}^{N_r} u_j \mathbf{E}_j \right) \mathbf{S}_{k-1} \left(\mathbf{I} + \sum_{j=1}^{N_s} s_j \mathbf{D}_j \right) \times \mathbf{R}_{k-1} \left(\mathbf{I} + \sum_{j=1}^{N_r} r_j \mathbf{E}_j \right) \mathbf{p}_{\mathbf{t}i} - \mathbf{m}_{\mathbf{t}i} \right\|_2^2 \tag{3.5}$$

with $\mathbf{c} \triangleq \{u_1, ..., u_{N_r}, s_1, ..., s_{N_s}, r_1, ..., r_{N_r}\}^T$ consisting of N_r reflection, N_s scale and N_r rotation variables. $\mathbf{U}_{k-1}$, $\mathbf{S}_{k-1}$ and $\mathbf{R}_{k-1}$ are the reflection, rotation and anisotropic scale matrices applied at the previous iteration of the procedure. Only an update to these matrices is found iteratively to better align the data set to the generic shape. This is done using the linearised basis $\mathbf{E}_j$ of the special orthogonal group representation discussed in Section B.2. $\mathbf{D}_j$ is the set of bases of a diagonal matrix with the only non-zero entries at $D_{jj} = 1$.

Application

The affine iterative closest point procedure as outlined in this chapter was implemented in Python [8]. The elastic surface registration procedure used by Bryan *et al.* [19] is applied to the registration of femur geometries in their article. For this reason, two femur surface meshes are obtained from the INRIA model shape repository [4] to illustrate the accurate implementation of this procedure.

One of the femur geometries obtained is from a right and the other from a left femur. The one femur is first reflected so that both represent the same side. The one model's axis is then transformed so both femur shapes are approximately aligned.

Before performing the rigid registration on the femur geometries, both models were translated so their nodal center lay on the origin of the Cartesian coordinate axis. This position is then used as the starting position for registration, as seen in Figure 3.1 (a) and 3.2 (a). From this starting position, the following two rigid registrations are performed:

- The first registration is applied only allowing rotation and translation. For this procedure, all three scale variables are constrained at a value of 1.

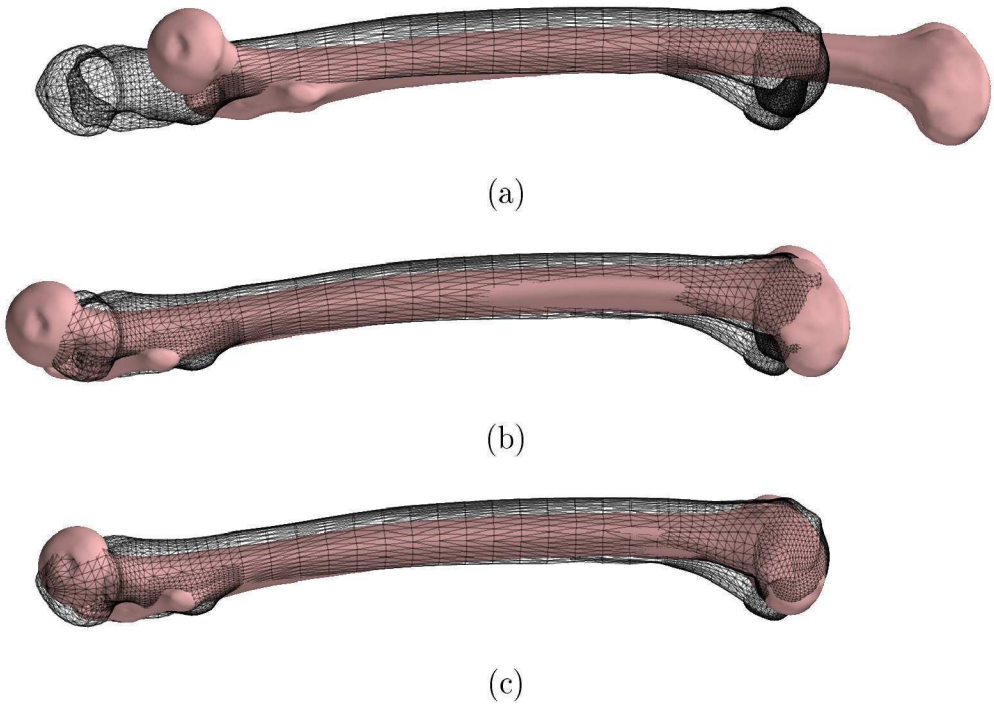

Figure 3.1: Lateral view of rigid registration results on two femur geometries obtained from the INRIA shape repository [4]. (a) Initial relative position and alignment of the two femurs. From this starting position, the rigid registration result is obtained by ICP for (b) rotation and translation only and (c) allowing isotropic scaling in addition to rotation and translation.

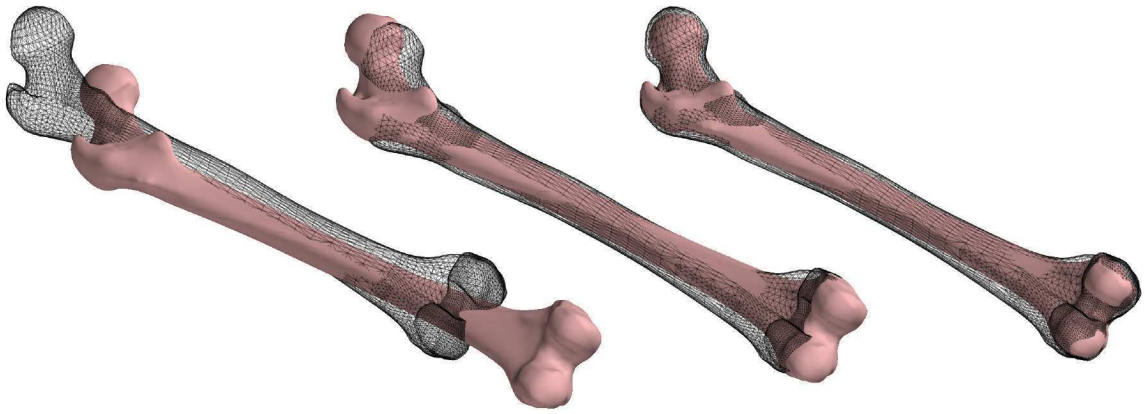

(a) (b) (c)

Figure 3.2: Isometric view of rigid registration results on two femur geometries obtained from the INRIA shape repository [4]. (a) Initial relative position and alignment of the two femurs. From this starting position, the rigid registration result is obtained by ICP for (b) rotation and translation only and (c) allowing isotropic scaling in addition to rotation and translation.

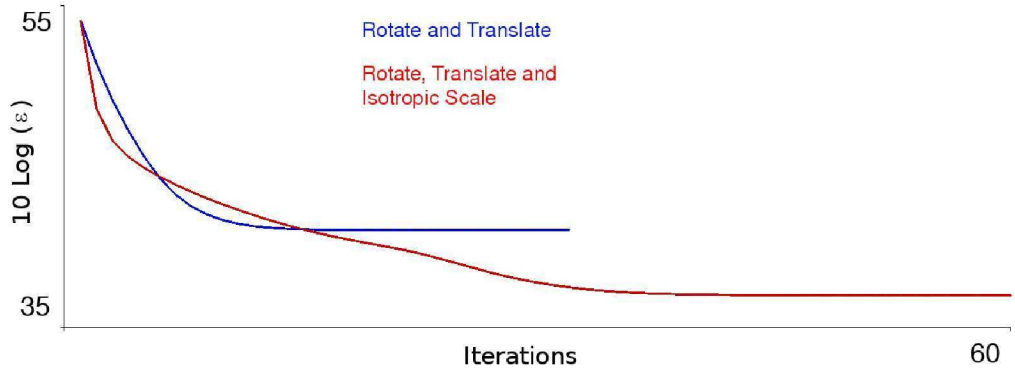

Figure 3.3: Convergence rate of the ICP. The blue line is obtained when only allowing rotation and translation while the red line is the convergence rate when rotation, translation and isotropic scale is allowed. At each iteration, ε is the function value after performing the least squares optimisation in Equation (3.5).

- The second registration is performed using an isotropic scale affine ICP with scale variables constrained to be within the bounds $[0.7, 1.2]$. These bounds were selected arbitrarily for this example and the optimisation is done with the additional requirement that all scale variables be equal.

The results of these rigid registrations on the femur geometries are visible in Figures 3.1 and 3.2. Anisotropic scaling is not considered in this report as the actual shape of the target should remain unchanged. The convergence rates of the affine ICP and isotropic scale affine ICP results of Figures 3.1 and 3.2 are visible in Figure 3.3.

3.2 Elastic Surface Registration

The elastic surface registration procedure of Moshfeghi *et al.* [44] as implemented and improved by Bryan *et al.* [19] is discussed in this section. They used this registration procedure to analyse the performance of orthopaedic implants while accounting for inter-patient variability in bone quality and geometry.

The creation of a three dimensional, statistical, finite element analysis ready model of a femur was achieved by Bryan *et al.* [19] via a registration scheme based on elastic surface matching and mesh morphing.

Establishing a correspondence between each member of the training set requires initially registering a common baseline mesh to each femur model surface. To do this, the target geometries are first aligned to the generic model using an ICP procedure [13]. After rigid registration is performed, surface matching iteratively deforms the baseline mesh vertices to better match the target surface.

In the registration procedure used by Bryan *et al.* [19], a smooth and accurate final mesh is obtained through user defined inputs that control the magnitude and speed of deformation. The registration is refined at each iteration through these user specified parameters. Initially the deformations have greater support, roughly aligning the surfaces before decreasing the support radius for finer local mesh deformations.

3.2.1 Registration Procedure

The elastic surface registration as used by Bryan *et al.* [19] is outlined in this subsection. Two meshes are taken as an input with $\mathcal{M}$ the generic surface and

$\mathcal{P}$ the target surface. These two meshes don't have to have the same number of degrees of freedom or connectivity. The generic surface is deformed iteratively to better represent the target geometry without its connectivity being affected.

The data and generic surface mesh is represented as

$$\mathcal{P} \triangleq \left\{ \left\{ \begin{array}{ccc} x_{p_i} & y_{p_i} & z_{p_i} \end{array} \right\}_{i=1}^{N_p}, \{\triangle_c\}_{c=1}^{T_p} \right\} \tag{3.6}$$

and

$$\mathcal{M} \triangleq \left\{ \left\{ \begin{array}{ccc} x_{m_j} & y_{m_j} & z_{m_j} \end{array} \right\}_{j=1}^{N_m}, \{\triangle_d\}_{d=1}^{T_m} \right\}. \tag{3.7}$$

In this representation, $\left\{ \begin{array}{ccc} x_{p_i} & y_{p_i} & z_{p_i} \end{array} \right\}$ is the i^{th} vertex of the target surface with N_p vertices. $\triangle_c$ refers to triangle patch c of which there is a total of T_p representing the target surface for example. Key steps to deform $\mathcal{M}$ into $\mathcal{P}$ are as follows:

- Registration inputs are specified. These include the target mesh $\mathcal{P}$ and base mesh $\mathcal{M}$. Other user specified parameters are a nearest neighbour parameter n, smoothing parameters γ, σ_0 and f, maximum number of iterations k_{max} and stopping criterion tolerance ε_T.

- Coarse registration with ICP is performed to align the target geometry to the generic mesh.

- The iteration counter and deformable surface is initialised so that $k = 1$ and $\mathcal{W}^{k-1} = \left\{ \begin{array}{ccc} x_{m_j} & y_{m_j} & z_{m_j} \end{array} \right\}_{j=1}^{N_m}$. Registration is performed while $k \leq k_{max}$:

  - Four $k-d$ tree representations are constructed. This is done for the centroids of surface triangulations and nodal coordinates of both $\mathcal{W}^{k-1}$ and $\mathcal{P}$.

  - For each node $\mathbf{w}_j$ in $\mathcal{W}^{k-1}$, $j \in \{1, 2, ..., N_m\}$, a registration to the target surface is determined. This can be better understood by also consulting Figure 3.4.

    * Using the $k-d$ tree representation of the target surface triangle centroids, the n nearest target triangles to $\mathbf{w}_j$ are determined.
    * The location of a registration point on these closest triangles are determined. This point $\mathbf{r}_{w_j}$, is produced by drawing a line from the point $\mathbf{w}_j$ perpendicular to the plane of each registered triangle. A

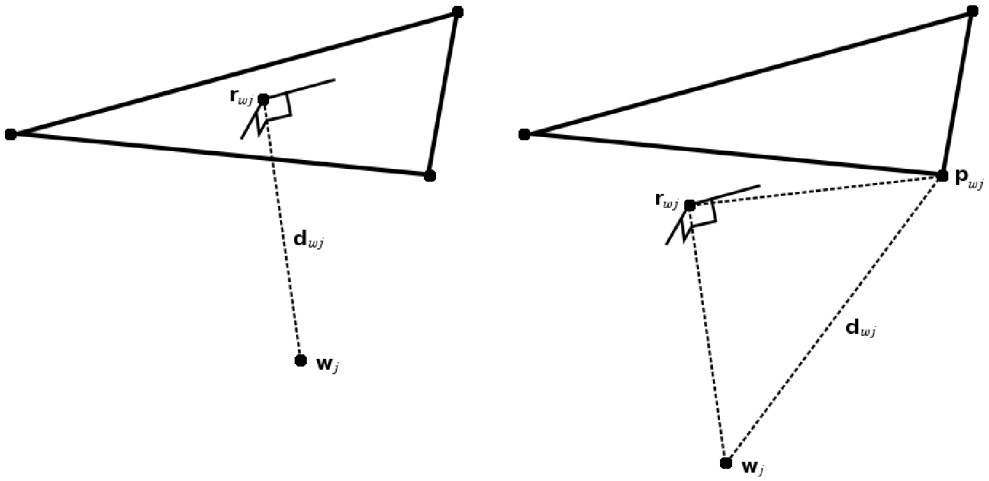

(a) (b)

Figure 3.4: Determining the registration of a point $\mathbf{w}_j$ onto one of the n closest triangles with (a) the registered point inside and (b) outside of the triangle boundary.

distance measure is then assigned to these triangles. If the point $\mathbf{r}_{w_j}$ lies inside a triangle, the distance measure is computed as $\left|\mathbf{r}_{w_j} - \mathbf{w}_j\right|$. Alternatively, if the point lies outside the triangle the distance measure is computed as $\left|\mathbf{r}_{w_j} - \mathbf{w}_j\right| + \left|\mathbf{p}_{w_j} - \mathbf{r}_{w_j}\right|$, where $\mathbf{p}_{w_j}$ is the closest vertex of that triangle to point $\mathbf{w}_j$.

* Inspecting all these distance measures for all n closest triangles, the closest triangle to point $\mathbf{w}_j$ is obtained. Using only this closest triangle, the required displacement to the target surface is determined. If the point $\mathbf{r}_{w_j}$ lies inside the closest triangle, the displacement is calculated as $\mathbf{d}_{w_j} = \mathbf{r}_{w_j} - \mathbf{w}_j$. Alternatively, if the point lies outside the triangle the displacement is calculated as $\mathbf{d}_{w_j} = \mathbf{p}_{w_j} - \mathbf{w}_j$.

– This registration procedure is then done again for the $\mathcal{P}$ onto $\mathcal{W}^{k-1}$. For each node $\mathbf{p}_i$ in $\mathcal{P}$, $i \in \{1, 2, ..., N_p\}$, a displacement to the deformable surface is determined as $\mathbf{d}_{p_i} = \mathbf{r}_{p_i} - \mathbf{p}_i$ if the point $\mathbf{r}_{p_i}$ lies inside the closest triangle or $\mathbf{d}_{p_i} = \mathbf{m}_{p_i} - \mathbf{p}_i$ if the point $\mathbf{r}_{p_i}$ lies outside the closest triangle.

– Having registered $\mathcal{W}^{k-1}$ onto $\mathcal{P}$ and $\mathcal{P}$ onto $\mathcal{W}^{k-1}$, a smooth displacement

field is computed for a point $\mathbf{x}$ as

$$S^{k-1}(\mathbf{x}) = \frac{1}{\gamma}\left[\frac{\sum_{j=1}^{N_m} G\left(\|\mathbf{x}-\mathbf{w}_j\|\right)\mathbf{d}_{w_j}}{\sum_{j=1}^{N_m} G\left(\|\mathbf{x}-\mathbf{w}_j\|\right)} - \frac{\sum_{j=1}^{N_m} G\left(\|\mathbf{x}-\mathbf{r}_{p_i}\|\right)\mathbf{d}_{p_i}}{\sum_{j=1}^{N_m} G\left(\|\mathbf{x}-\mathbf{r}_{p_i}\|\right)}\right]. \quad (3.8)$$

In Equation (3.8), $G(d)$ is the Gaussian weighting function suggested by Moshfeghi [44]:

$$G(d) = e^{-d/\sigma_k^2}, \quad (3.9)$$

where d is a positive scalar distance measure. The smoothing parameter σ_k is decreased at each iteration allowing for more compact support using the update $\sigma_k = \sigma_0 f^{-k}$ with $1 \leq f \leq 2$.

- The deformable surface is updated as

$$\mathcal{W}_j^k = \mathcal{W}_j^{k-1} + S^{k-1}(\mathbf{w}_j). \quad (3.10)$$

- To prevent mesh folding, Bryan *et al.* [19] preformed a set number of improved Laplacian smoothing iterations to the deformable mesh $\mathcal{W}_j^k$ before performing another registration iteration.
- Convergence is determined on the average total deformation applied for the current iteration and the solution is terminated if

$$\varepsilon = \frac{1}{N_m}\sum_{j=1}^{N_m}\left|S^{k-1}(\mathbf{w}_j)\right| \leq \varepsilon_T. \quad (3.11)$$

In their study, Bryan *et al.* [19] used a nearest neighbour parameter $n = 50$, the smoothing parameters $\gamma = 2$, $\sigma_0 = 10$ and $f = 1.0715$ and the maximum iterations k_{max} set to 100 when registering the femur geometries. Bryan *et al.* [19] report that setting up a greater similarity measure in registration could result in mesh folding.

The updated nodal coordinates of the generic mesh is returned after reaching a stopping criterion. This stopping criterion could either be the satisfaction of Equation (3.11) or that the maximum number of iterations is reached.

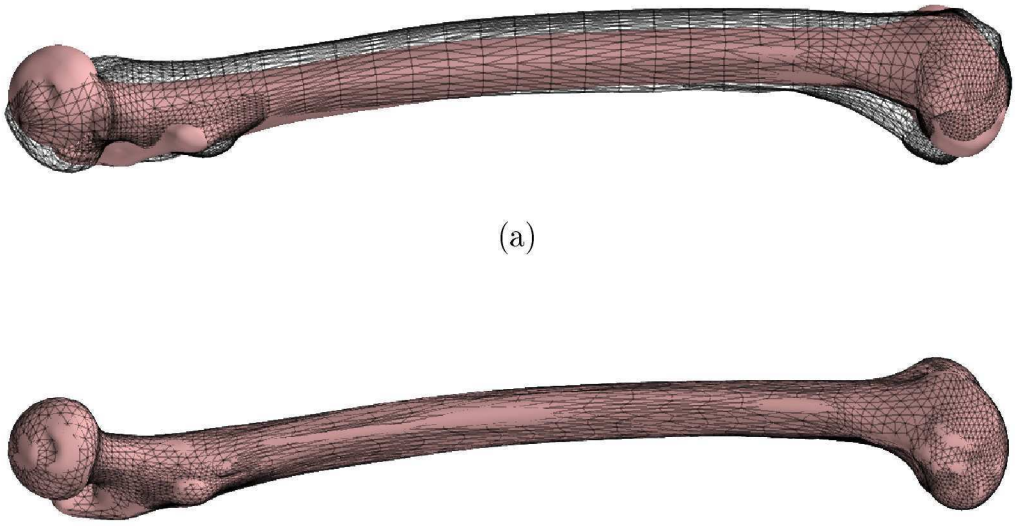

(a)

(b)

Figure 3.5: Elastic registration on the isotropic scale ICP result. (a) Lateral view of the rigid registration result on the two femur geometries. (b) Lateral view of the elastic surface registration result to deform the black wire-frame mesh into the target geometry at iteration 100.

3.2.2 Application

Registration on Femur Geometries

The elastic surface registration is implemented in Python. The performance of this registration procedure with the same parameter values as used by Bryan *et al.* [19] on the two femur surface meshes is visible in Figures 3.5 and 3.6.

The isotropic scale rigid registration result is used as the starting position of the elastic surface registration procedure. The chosen generic surface model is deformed to best fit the other geometry. From the figures illustrating this result, no real problem in registering these geometries are noticed.

The effect of selecting various registration parameters on the obtained result is visible in Figures 3.7 and 3.8. This analysis is done to determine the sensitivity of the registration result to user controlled inputs. To obtain the convergence plot in Figure 3.7 (a), the smoothing parameter γ is varied while the other parameters are kept as used by Bryan *et al.* [19]. This is then done again for a varying σ_0

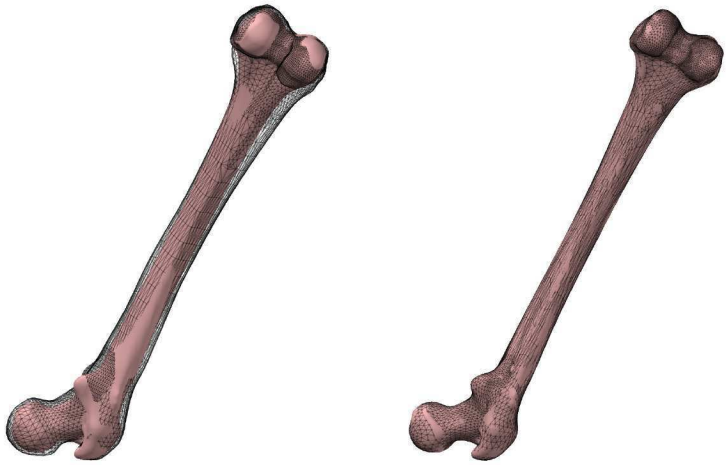

(a) (b)

Figure 3.6: Elastic registration on the isotropic scale ICP result. (a) Isometric view of the rigid registration result on the two femur geometries. (b) Isometric view of the elastic surface registration result to deform the black wire-frame mesh into the target geometry at iteration 100.

and varying f in Figures 3.7 (b) and (c). These figures show the convergence of ε in Equation (3.11) subject to these varying parameters for the femur registration problem.

The effect of performing 10 Taubin [61] smoothing iterations after every 5 elastic registration iterations is visible as the jumps in these figures. The smoothing done in the implemented procedure is chosen for it's ability to reduce high frequency surface noise without compromising subject volume. It is an enhanced version of Laplacian type smoothing.

Bryan *et al.* [19] mention the need for smoothing to prevent mesh folding and maintain a good quality mesh. Unfortunately the smoothing type and frequency of application is not mentioned. The spikes visible in Figure 3.7 seem to happen at a stage in the procedure where very localised deformations are applied. These very localised deformations likely resemble high frequency surface noise and can be largely undone by applying a few smoothing iterations.

Using the convergence plots of Figure 3.7, four of the deformed meshes are selected and shown in Figure 3.8 to inspect how close the registration came to represent the target femur geometry. The four meshes are obtained as follow:

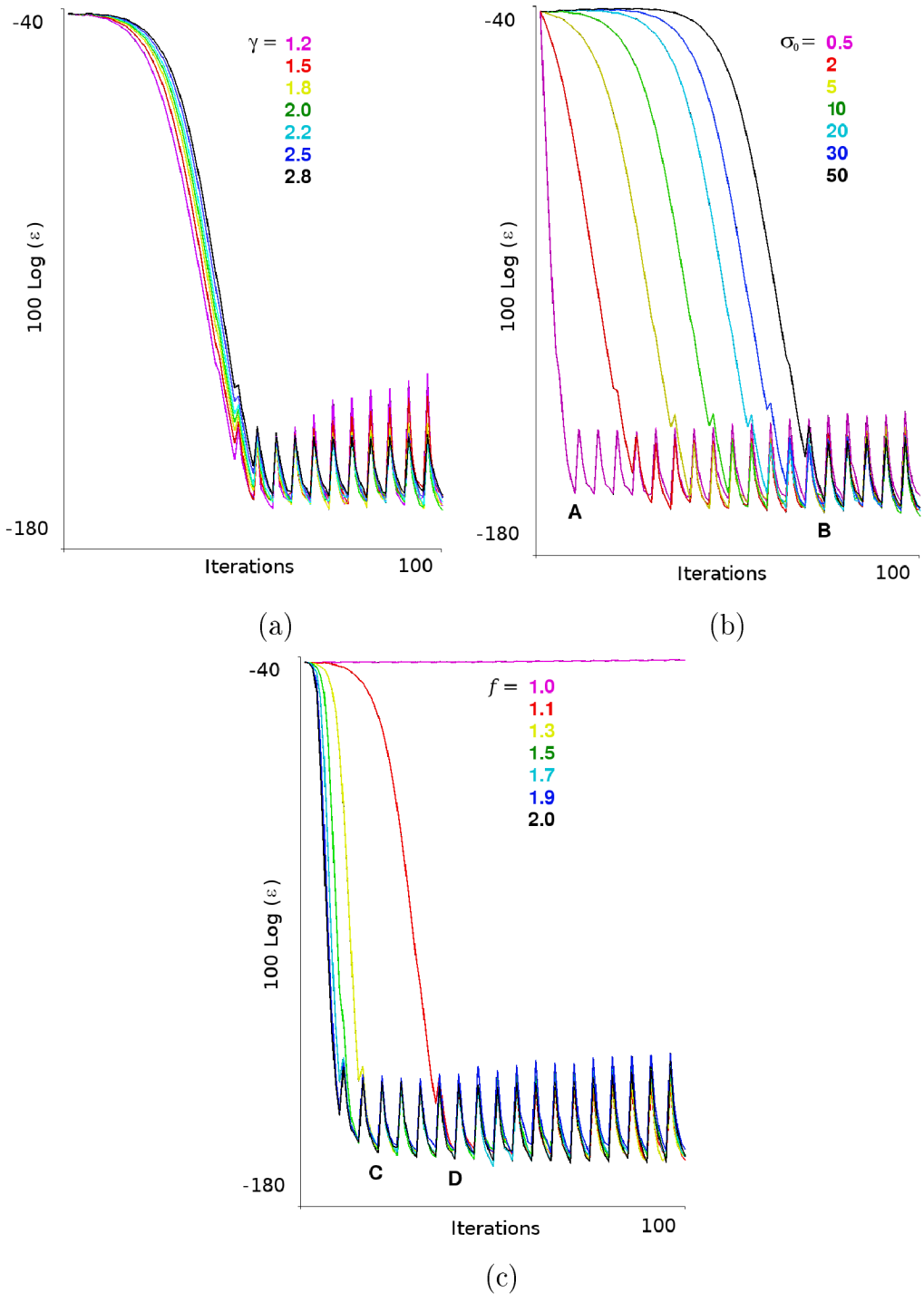

Figure 3.7: Improvement on the average deformation similarity criteria in Equation (3.11) subject to varying user controlled parameters. (a) $\sigma_0 = 10$ and $f = 1.0715$ while varying γ. (b) $f = 1.0715$ and $\gamma = 2$ while varying σ_0. (c) $\sigma_0 = 10$ and $\gamma = 2$ while varying f.

(a)

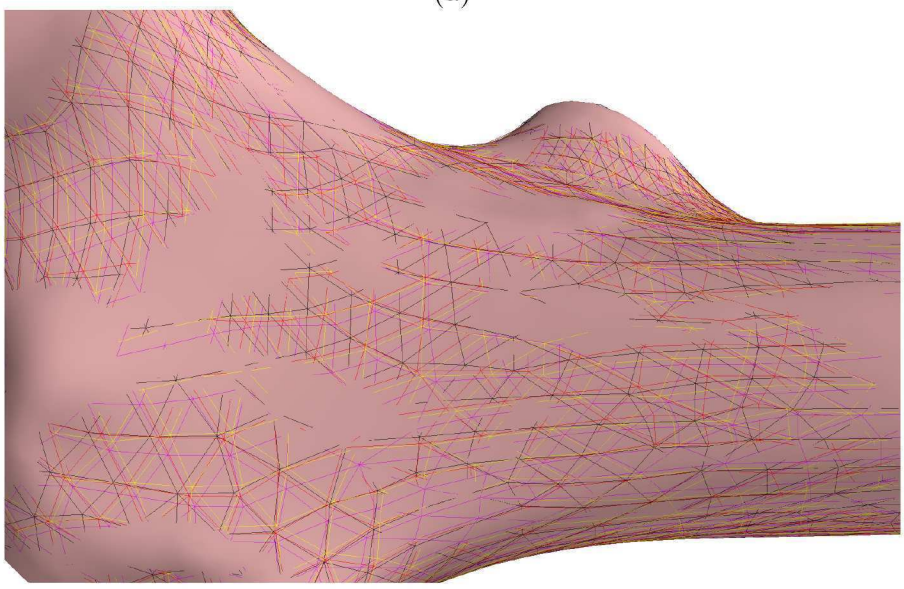

(b)

Figure 3.8: Various deformed generic surface target representations obtained with different user controlled parameters. Mesh **A** is the registration result with the parameters set to $\gamma = 2$, $\sigma_0 = 0.5$ and $f = 1.0715$ at 10 registration iterations. Mesh **B** is the registration result with the parameters set to $\gamma = 2$, $\sigma_0 = 50$ and $f = 1.0715$ at 75 registration iterations. Mesh **C** is the registration result with the parameters set to $\gamma = 2$, $\sigma_0 = 10$ and $f = 1.3$ at 20 registration iterations. Mesh **D** is the registration result with the parameters set to $\gamma = 2$, $\sigma_0 = 10$ and $f = 1.1$ at 40 registration iterations. The average total deformation plots in Figure 3.7 also indicate where meshes **A** - **D** are chosen.

- Mesh **A** is the registration result with the parameters set to $\gamma = 2$, $\sigma_0 = 0.5$ and $f = 1.0715$ at 10 registration iterations.
- Mesh **B** is the registration result with the parameters set to $\gamma = 2$, $\sigma_0 = 50$ and $f = 1.0715$ at 75 registration iterations.
- Mesh **C** is the registration result with the parameters set to $\gamma = 2$, $\sigma_0 = 10$ and $f = 1.3$ at 20 registration iterations.
- Mesh **D** is the registration result with the parameters set to $\gamma = 2$, $\sigma_0 = 10$ and $f = 1.1$ at 40 registration iterations.

Out of this analysis done on the sensitivity of the registration result to user selected registration parameters, it is apparent that a target representation result obtained with this method is not unique. The four deformed femur meshes all seem to adequately represent the target surface with a wide range of different final nodal coordinates as visible in Figure 3.8 (b).

The parameters σ_0 and f influence the effective radius of the Gaussian smoothing function given in Equation (3.9). The smoothing parameter σ_0 is the initial support radius and therefore a smaller value would allow local deformations faster while a larger initial value would help account for initial global misalignment. This is visible as the small gradient in the first few iterations of the convergence plots. The effect of choosing the initial support radius $\sigma_0 = 10$ depends on the overall scale of the deformable and target mesh. If the meshes were now scaled with a factor of 10 before repeating the analysis, the effect of $\sigma_0 = 10$ would be the same as using $\sigma_0 = 1$ in the original analysis.

The parameter f in addition affects the rate at which the effective Gaussian support radius decays. A larger parameter forces localised deformation at an earlier stage where the choice of parameter $f = 1$ may be understood as a constant Gaussian support radius for all iterations. The deformation applied at each iteration with $f = 1$ is repeatedly determined using the initial support radius σ_0 .

The parameter γ in Equation (3.8) simply has an effect on the amount of smooth deformation field calculated that is applied to the deformable mesh. Using the suggestion of the paper by Bryan *et al.* [19], this parameter set to $\gamma = 2$ simply implies that half of the computed deformation at each iteration is applied to the deformable mesh.

Registration on Skull Geometries

The implemented procedure is applied to the creation of a symmetric skull representation. This symmetric skull will be used as the generic mesh and deformed into representations of the two skull geometries used in the initial FEA.

To create a symmetric generic skull form, a cleaned and smoothed version of the prognathic skull form is used as the basis on which this generic form is built. The orientation of this smoothed skull is first updated so that it best matches it's reflected mesh. The original position of the smooth skull surface in relation to it's reflection is given in Figure 3.9. The position of the smoothed skull is then updated using the ICP procedure in the following way:

- An iteration of the ICP procedure is performed allowing only rotation and translation.
- The average of the nodal coordinates in their previous and current position is determined and set as the new skull position.
- The target is updated as the reflected skull surface of the new skull position before another iteration is performed.

The result after rotating and translating the smoothed skull surface to best fit it's reflection is visible in Figure 3.10. To then create a symmetric version of the cleaned and smoothed skull, an elastic registration from the skull to it's reflection is first required. If the registration is adequate, the average between the undeformed and deformed mesh should result in a symmetric version. This symmetric skull shape could then be used as the generic mesh in subsequent registrations to geometries in the statistical sample of skull shapes.

While deforming the smooth skull into it's reflection, a few problems appear in the result obtained with the original procedure. One such problem is highlighted in the cut planes depicted in Figure 3.11. The overlapping sinuses create a problem in elastic registration where a closest point on the opposite mesh is used to determine a registered position. To solve this problem, Chapter 4 focuses on the extraction of features on a surface mesh. These features are extracted with the aim of using an additional feature based registration.

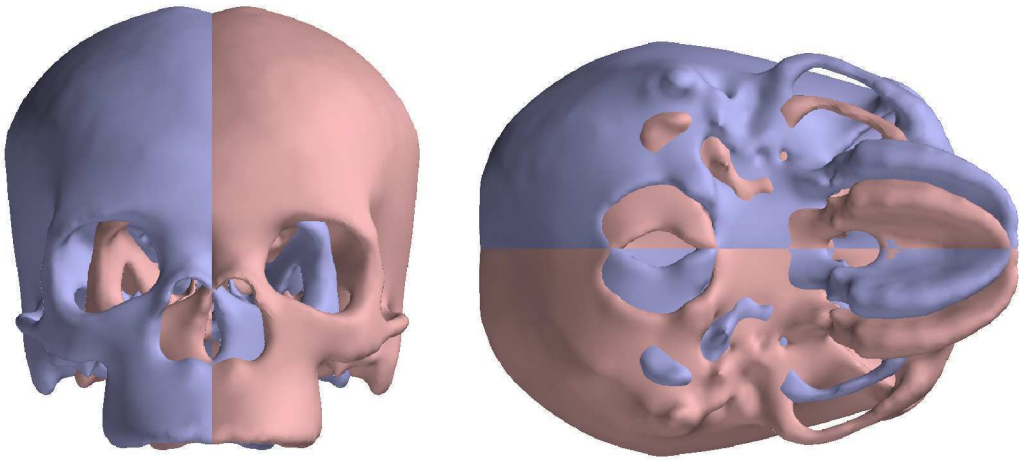

(a) (b)

Figure 3.9: Initial position of the smoothed skull mesh and it's reflection.

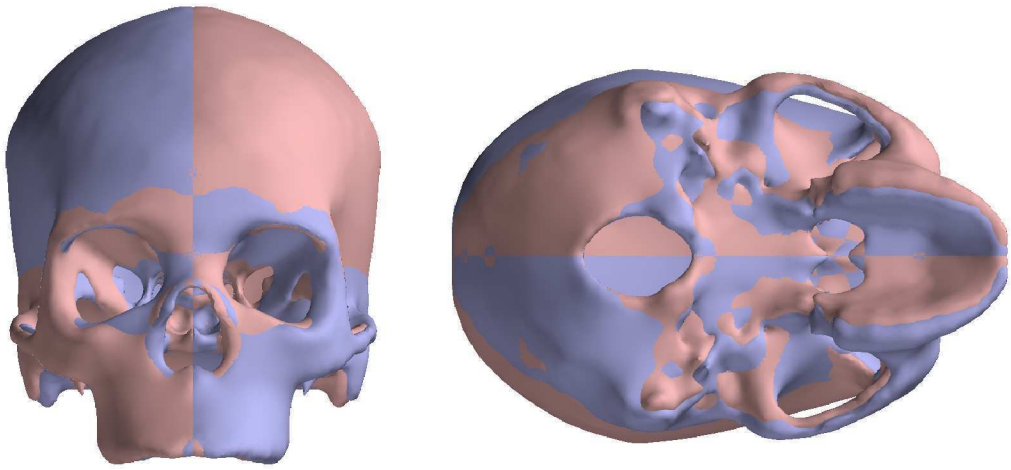

(a) (b)

Figure 3.10: Initial position of the smoothed skull mesh and it's reflection.

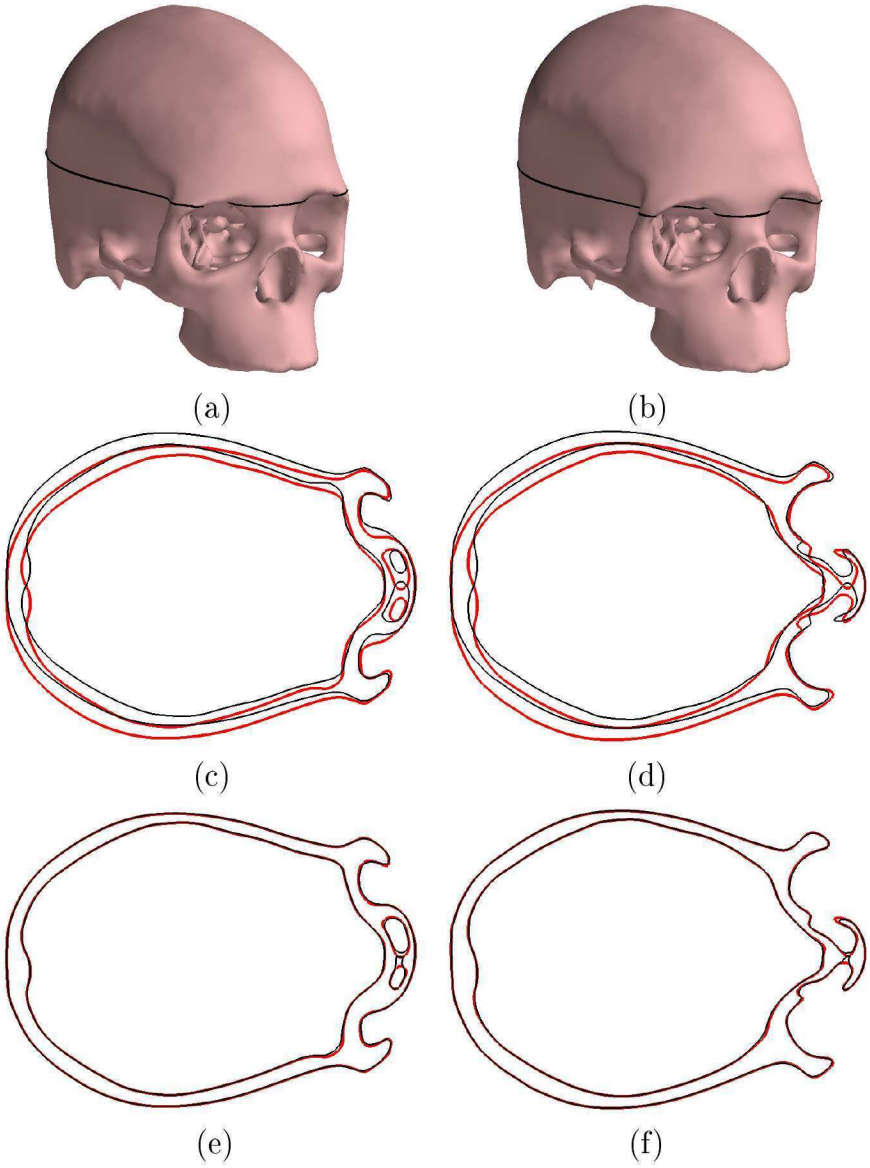

Figure 3.11: Problems with the sinus in elastically registering the smooth skull mesh into its reflection. (a) Position of cut plane (c) and (e). (b) Position of cut plane (d) and (f). (c), (d) Initial position of deformable mesh in relation to the target (The blue mesh in Figure 3.10 is set as the deformable mesh and is registered onto it's reflection). (e), (f) Elastic registration result at iteration 100. The red line represents the position of the target surface in that plane and the black line the deformable mesh surface.

3.3 Remarks and Conclusions

Apart from the questionable uniqueness of a registration result, additional alterations to the procedure are also required in order to compare the masticatory induced stresses in various skull forms. Where surfaces overlap, it is possible to obtain a registration of the deformable surface to sections on the target surface that are visibly invalid.

The possibility of this invalid registration is visible in the initial attempt to create a symmetric skull mesh for use as a generic mesh surface. This generic surface will be deformed into representations of the two skull geometries used in the initial FEA.

If a more rigorous approach is followed to first ensure corresponding feature registration, this could be done in conjunction with the elastic surface registration procedure implemented to possibly obtain better registration results. Again referring to Figure 3.11, it is decided that at least some kind of usable representation is required for this initial work into elastic registration using the implemented procedure. It was decided that the remainder of the work done for this report would be focused on incorporating feature based registration along with the implemented surface registration. This would be done in a way that complements the surface registration procedure and wouldn't necessarily improve on the uniqueness of the registration result.

The uniqueness of the registration result would necessarily affect the accuracy with which the modes of variation are represented using the implemented procedure. It also implies an uncertainty in claiming one-to-one correspondence between various shapes and the accurate mapping of one surface onto another which is not ideal. The final results obtained on the difference in stress field for the varying skull geometries would therefore simply be considered the maximum possible difference due to the inherent uncertainty.

The accuracy with which the registration is performed could form the basis of subsequent research. A unique and path independent registration result could perhaps be achieved through a better defined optimisation procedure, but this would not be addressed in the current work.